Laser Powder Bed Fusion of Bismuth Telluride: Process-Structure-Property Relationships

Cagri Oztan[1], Eric Fodran[2], Eric Barnes[2], Saniya LeBlanc[1]*

[1] The George Washington University, Department of Mechanical and Aerospace Engineering
800 22nd St. NW, Suite 3000, Washington, DC 20052, USA

[2] Northrop Grumman Aerospace Systems, El Segundo, CA, USA

*E-mail: sleblanc@gwu.edu

Abstract

Thermoelectric generators possess a vast potential for waste heat recovery. Yet, the traditional fabrication methods of thermoelectric structures suffer from material loss and are limited to planar geometries. As a solution, laser additive manufacturing of thermoelectric materials has attracted considerable attention. In this research, the process-structure-property relationship of laser processed bulk bismuth telluride parts has been explored. Under constant laser power and scan speed, the effects of variation in scan pattern, number of scans, hatch spacing and layer height on the microstructural and thermoelectric properties were investigated. It was concluded that the laser powder bed fusion enables formation of intensive interfaces with preferential grain growth and certain scan patterns result in enhancement in relative density and thermoelectric properties.

1. Introduction

Thermoelectric generators offer the potential for effective waste-heat recovery and reliable and silent power generation for a wide range of applications [1]. The efficiency of a thermoelectric (TE) material is characterized by dimensionless figure of merit, *ZT*, which is defined as $ZT=(S^2\sigma T/k)$, where S, σ, T and k denote Seebeck coefficient, electrical conductivity, absolute temperature, and thermal conductivity, respectively. For a TE material to be considered efficient, high-power factor ($S^2\sigma$) and low thermal conductivity (k) must be achieved at a certain temperature.

As a drawback, traditional thermoelectric generator manufacturing uses bulk material processing with assembly and integration steps which lead to performance degradation, material loss and limited geometries. Typical semiconductor materials processing is not conducive to making energy devices like thermoelectric generators: it is limited to thin film, micro/nanofabrication techniques such as deposition and photolithography [2]. It is ideal for achieving good resolution of micro/nanoscale features but is not suitable for large-area processing and components with thick/bulk material form factors such as thickness, geometric, and structural variations on the scale of hundreds of microns to millimeters [3]. To tackle these limitations, additive manufacturing of thermoelectric semiconductors has recently emerged since it enables novel, three-dimensional structures which are otherwise difficult and expensive to achieve through traditional manufacturing techniques [4].

As an additive method, laser powder bed fusion (LPBF, also termed as selective laser melting) locally melts successive layers of material powder using a laser beam to construct three-dimensional objects. The method has been investigated several times and has shown promising

results that would enable new geometries and architectures, material-to-device integration, and large-area processing for thermoelectric structures [5-7]. However, the advancement necessitates fundamental investigations of the nano-, micro-, and meso-scale structures that form based on varying laser processing parameters as well as the impact of those multi-scale structures on the thermoelectric properties of the final part. Moreover, due to their inherently low thermal conductivities and brittle fracture properties, laser-processing of thermoelectric materials requires special attention to explore their unique process-structure-property relationship.

As the result of a collaboration between The LeBlanc Lab at The George Washington University and the Northrop Grumman team, this work aimed to characterize the relationship between laser processing parameters (e.g., laser power, scan speed, hatch spacing), the resultant multi-scale structures (e.g., density, melt zone, porosity, grain morphology), and the thermoelectric properties (e.g., Seebeck coefficient, electrical conductivity) of bismuth telluride (Bi_2Te_3) material, which was successfully laser processed before [8-11].

2. Materials and Methods

Commercial, undoped Bi_2Te_3 powder was purchased from American Elements (CAS #: 1304-82-1). Due to the highly inconsistent particle sizes (**Figure 1A**) and the need for higher powder flowability during LPBF, sieving was performed to isolate particles smaller than 53 µm. Sieved powder was later used as the base material for LPBF. The powder was spread on a custom-built, micrometer-adjusted powder bed platform (**Figure 1B**) to fabricate bulk samples with a rectangular prism (15 mm x 2 mm) shape having thicknesses of at least 2 mm. These sample dimensions are required for the subsequent TE property characterization.

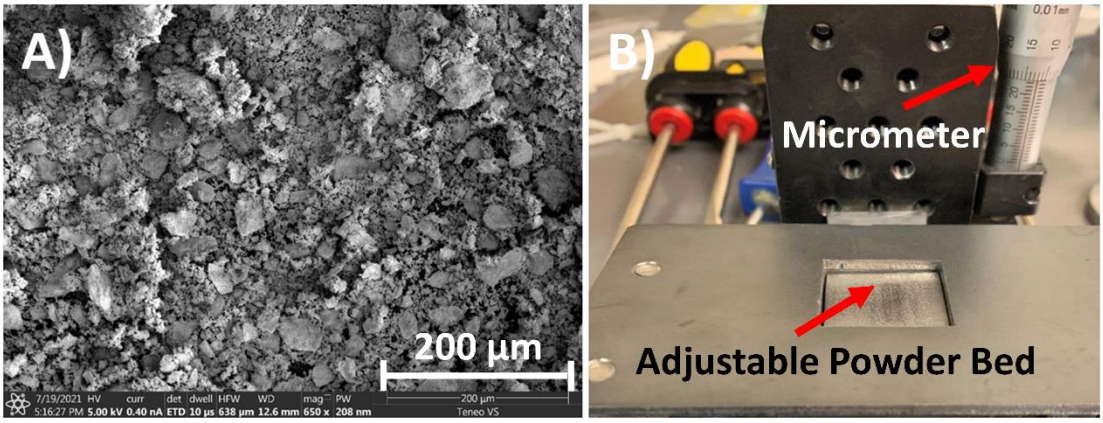

Figure 1: **A)** SEM image of the Bi_2Te_3 powder, **B)** Custom made powder bed platform

Bulk samples were fabricated using a custom LPBF setup (1070 nm, 50 µm spot size, 0–100 W YAG laser with an F-theta lens from IPG Photonics, CA, USA) in a weld chamber filled with high purity argon gas. The ambient oxygen level in the chamber was maintained at < 0.01%, which was monitored using a sensor at the top of the chamber. The laser raster was controlled using an integral galvanometer scanner. All bulk samples were processed under constant laser power and speed of 25 W and 350 mm/s, respectively. The altered parameters were layer height (100, 150 and 200 µm), hatch spacing (25 and 37.5 µm), scan pattern and number of scans (up to five). The illustrations of the scan patterns are provided in **Figure 2**.

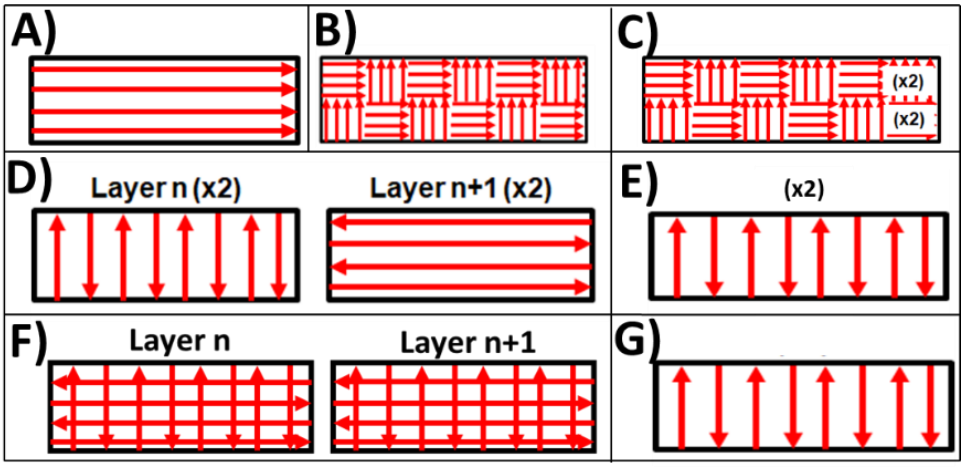

Figure 2: Scan patterns attempted in this project: **A)** Unidirectional, **B)** Chess Plane, **C)** Chess Plane (2 scans), **D)** Double-Perpendicular (2 scans), **E)** Double Vertical (2 scans), **F)** Double Rectangular, **G)** Vertical

The Seebeck coefficient and electrical conductivity were measured in a helium environment from room temperature to 150°C using a Linseis LSR-3. Characterized samples were later measured for density using a Mettler Toledo XS204 density determination kit. Finally, samples were cleaved along their cross sections and mounted in epoxy molds for polishing to reveal the microstructure. Polishing was done with an Allied HighTech #180-25015 equipment.

3. Results

3.1. Thermoelectric Property Characterization

Figure 3A provides the Seebeck coefficient data for the samples fabricated in this project. All samples other than the one scanned 5 times with unidirectional scanning pattern exhibited positive Seebeck coefficient. It can be inferred that, although scanning twice increases the Seebeck coefficient, additional scans cause a Seebeck coefficient reduction. **Figure 3B** displays the variation of electrical conductivity with temperature. It can be deduced that, certain scanning strategies result in a dramatic increase in the electrical conductivity. This increase will later be explained by the energy dispersive spectroscopy (EDS) measurements. **Figure 4** shows the calculated power factor ($S^2\sigma$) values. Double scanning corresponds to a substantial increase in power factor.

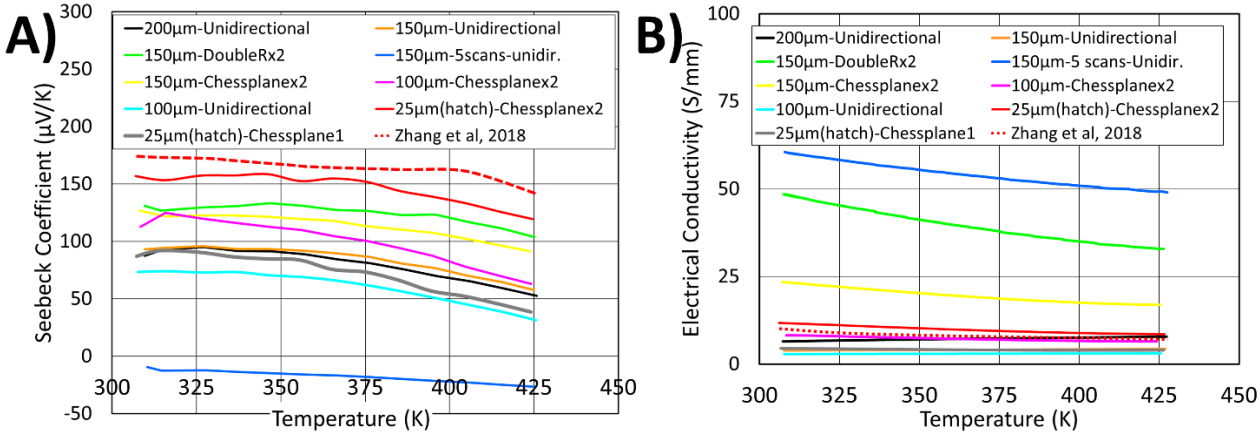

Figure 3: A) Variation of Seebeck coefficient (S) with temperature and comparison of the data with a previous publication where a single-scan unidirectional scan strategy was used [10]. **B)** Variation of electrical conductivity (σ) with temperature and comparison of the data with literature [10].

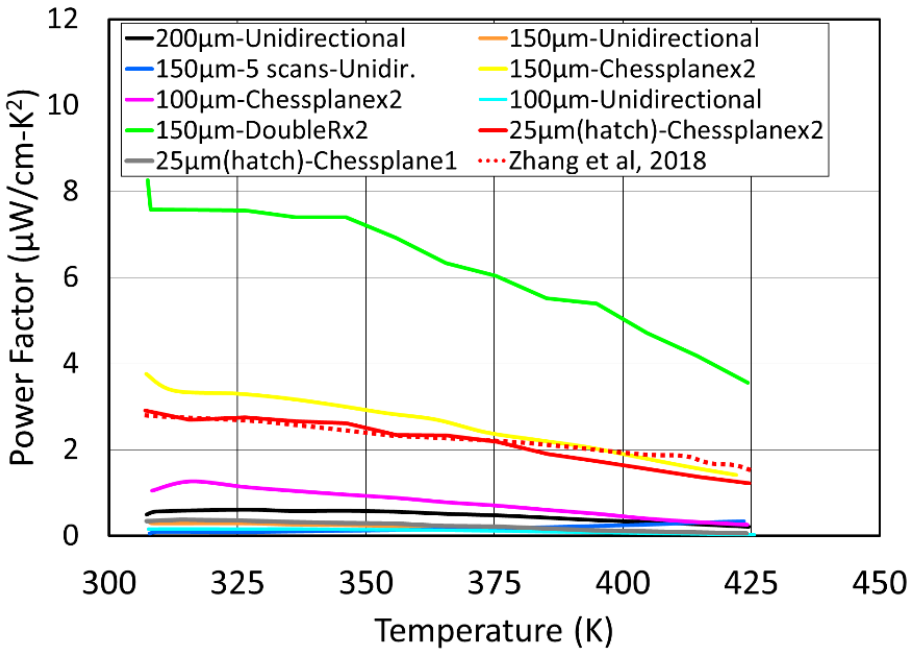

Figure 4: Variation of power factor ($S^2\sigma$) with temperature and comparison of the findings with the literature [10].

Thermoelectric characterization data shows that any deviation from the optimum layer height of 150 µm results in a loss in electrical conductivity. However, excessive rescanning even at the optimum layer height of 150 µm causes a reduction in the power factor. On the other hand, double rectangular and chess plane scanning patterns are more suitable strategies to achieve higher electrical conductivity.

3.2. Microstructural Characterization

Figure 5 shows the cross section of each polished sample under optical microscope polarized light; relative density of each sample is displayed on the image. The porosity in the samples may be attributed to the lack of fusion between the layers, along with the aspherical Bi_2Te_3 powder particles which resulted in insufficient powder flowability. In all samples, the unique microstructure of laser-processed parts with preferential grain growth can be observed. It is also evident that the samples with power factor possessed higher relative densities.

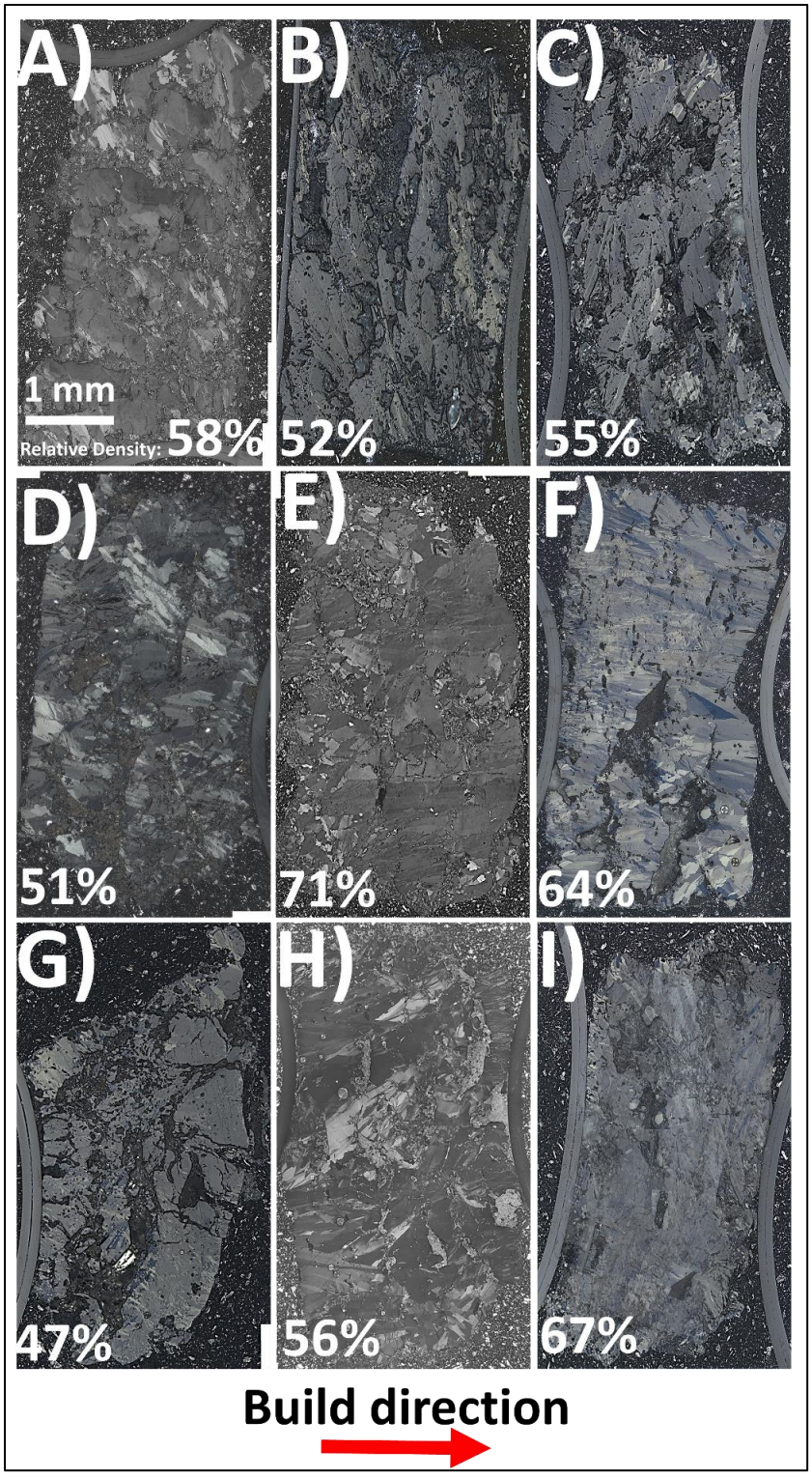

Figure 5: Polarized optical microscope cross sectional images of the bulk Bi_2Te_3 samples: A) 100 µm, double scan, chess plane, B) 200 µm, single scan, unidirectional, C) 150 µm, unidirectional, single scan, D) 100 µm, single scan, unidirectional, E) 150 µm, double scan, chess plane, F) 150 µm, double scan, double rectangular, G) 150 µm, 5 scans, unidirectional, H) 25 µm hatch spacing, single scan, chess plane, I) 25 µm hatch spacing, double scan, chess plane

SEM images of all samples are provided in **Figure 6.** In all samples, thermal cracking due to thermal cycles and porosity are observed. Such defects can be ascribed to cause the loss in electrical conductivity. The presence of the defects becomes more pronounced especially in the samples that had a layer height other than 150 µm. In all samples, the well-fused sections have minimal porosity.

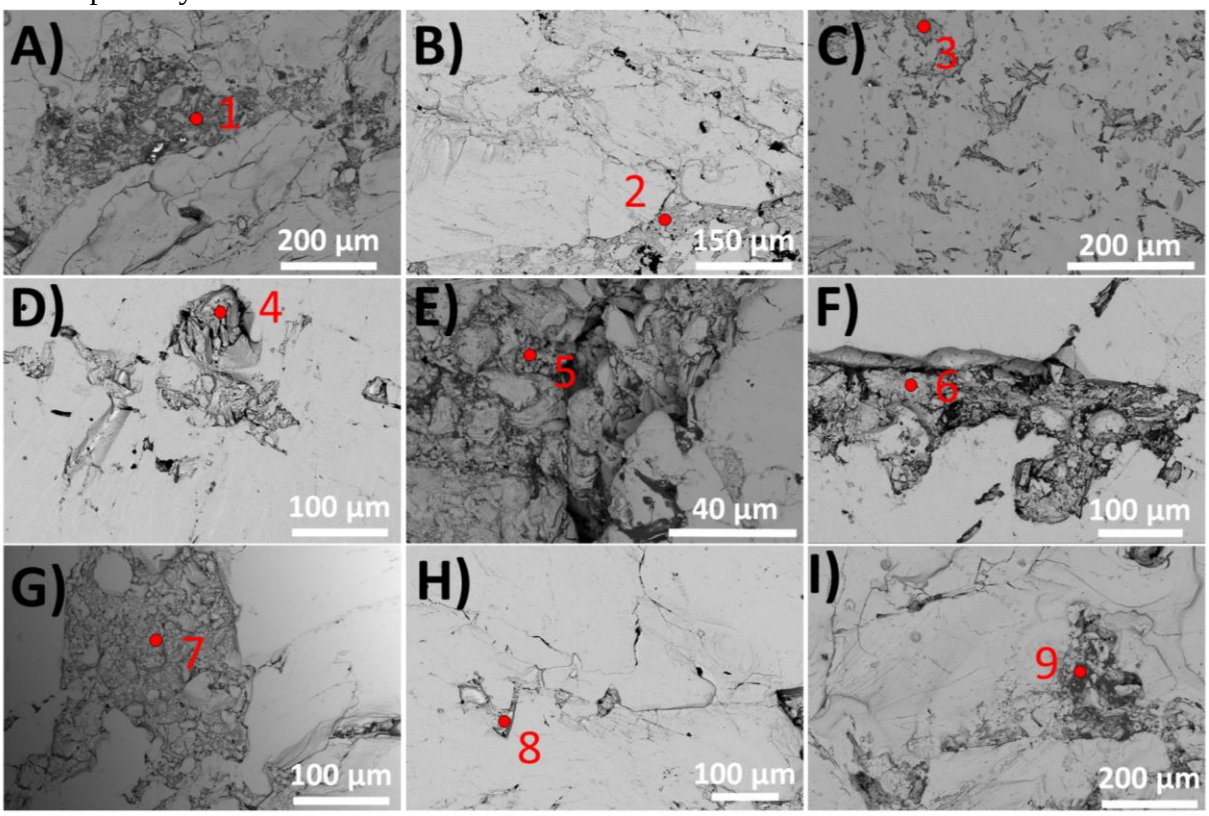

Figure 6: SEM images of the cross sections of the bulk Bi_2Te_3 samples: A) 200 µm, single scan, unidirectional, B) 150 µm, 5 scans, unidirectional, C)100 µm, single scan, unidirectional, D) 150 µm, double scan, chess plane, E) 150 µm, unidirectional, single scan, F) 150 µm, double scan, double rectangular, G) 100 µm, double scan, chess plane, H) 25 µm hatch spacing, double scan, chess plane, I) 25 µm hatch spacing, single scan, chess plane.

The results of the EDS analyses conducted on the points marked in Figure 6 are provided in **Table 2**. These points were selected due to the heavy presence of porosity around them. In well-fused sections of all samples, minimal deviation from stoichiometry was observed. Hence, the elemental compositions around the porous regions were observed to govern the resultant thermoelectric properties. Generally, the samples that exhibited high density had minimal oxidation and deviation from stoichiometry, which is in good agreement with their decent thermoelectric properties.

Table 2: EDS results in the corresponding points

EDS Point	O	Bi	Te	$Te_{at\%}/Bi_{at\%}$	Deviation from stoichiometry (%)
1	42.85	24.93	32.22	0.86	42.62
2	73.49	9.73	16.78	1.15	23.43
3	5.59	62.06	32.35	0.35	76.86

4	14.54	29.01	56.45	1.30	13.60
5	38.83	33.00	28.17	0.57	62.10
6	13.15	28.00	58.85	1.40	6.68
7	23.61	31.19	45.20	0.97	35.66
8	24.81	30.50	44.69	0.98	34.94
9	14.41	29.69	55.90	1.26	16.32

4. Conclusion:

In this project, we showed that microstructural and thermoelectric properties of laser processed bulk Bi_2Te_3 parts exhibited significant difference under varying hatch spacing, scan pattern, layer height and number of scans. The highest power factor was obtained using double rectangular scanning strategy with double scans, whereas the most consistent thermoelectric properties were observed using chess plane scan strategy. The maximum relative density in the bulk parts was 71%. Scanning electron microscopy analysis revealed that all samples exhibited minimum porosity and oxidation in the well-fused sections. However, the magnitude of deviation from stoichiometry in the porous regions heavily affected the resultant thermoelectric properties. On the other hand, excessive number of scans was observed to change the primary charge carriers, resulting in negative Seebeck coefficient. The findings in this work are expected to provide deeper insight into understanding the process-structure-property relationship of laser-processed semiconductors.

References

[1] Nolas, G.S., Sharp, J., and Goldsmid, J., "Thermoelectrics: basic principles and new materials developments," Vol. 45, Springer Science & Business Media, 2013,

[2] Velosa-Moncada, L.A., Raskin, J., Aguilera-Cortés, L.A., "Estimation of the Young's Modulus of Nanometer-Thick Films Using Residual Stress-Driven Bilayer Cantilevers," *Nanomaterials,* Vol. 12, No. 2, 2022, pp. 265.

[3] Fruncillo, S., Su, X., Liu, H., "Lithographic processes for the scalable fabrication of micro- and nanostructures for biochips and biosensors," *ACS Sensors,* Vol. 6, No. 6, 2021, pp. 2002-2024.

[4] Du, Y., Chen, J., Meng, Q., "Thermoelectric materials and devices fabricated by additive manufacturing," *Vacuum,* Vol. 178, 2020, pp. 109384.

[5] Chen, T., Luo, C., Yan, Y., "Rapid fabrication and thermoelectric performance of SnTe via non-equilibrium laser 3D printing," *Rare Metals,* Vol. 37, No. 4, 2018, pp. 300-307.

[6] Shi, J., Chen, X., Wang, W., "A new rapid synthesis of thermoelectric Sb2Te3 ingots using selective laser melting 3D printing," *Materials Science in Semiconductor Processing,* Vol. 123, 2021, pp. 105551.

[7] Thimont, Y., Presmanes, L., Baylac, V., "Thermoelectric Higher Manganese Silicide: Synthetized, sintered and shaped simultaneously by selective laser sintering/Melting additive manufacturing technique," *Materials Letters,* Vol. 214, 2018, pp. 236-239.

[8] El-Desouky, A., Read, A.L., Bardet, P.M., "Selective laser melting of a bismuth telluride thermoelectric materials," *Proc Solid Free Symp,* Solid Freeform Fabrication Symposium, Austin, Texas, 2015, pp. 1043-1050.

[9] El-Desouky, A., Carter, M., Mahmoudi, M., "Influences of energy density on microstructure and consolidation of selective laser melted bismuth telluride thermoelectric powder," *Journal of Manufacturing Processes,* Vol. 25, 2017, pp. 411-417.

[10] Zhang, H., Hobbis, D., Nolas, G.S., "Laser additive manufacturing of powdered bismuth telluride," *Journal of Materials Research,* Vol. 33, No. 23, 2018, pp. 4031-4039.

[11] Welch, R., Hobbis, D., Birnbaum, A.J., "Nano-and Micro-Structures Formed during Laser Processing of Selenium Doped Bismuth Telluride," *Advanced Materials Interfaces,* Vol. 8, No. 15, 2021, pp. 2100185.